REPORT DOCUMENTATION PAGE

1. REPORT DATE (DD-MM-YYYY)	2. REPORT TYPE	3. DATES COVERED (From - To)
09-10-2009	Book Chapter	

4. TITLE AND SUBTITLE	5a. CONTRACT NUMBER
Fourier, Seattering, and Wavelet Transforms: Applieations to Internal Gravity Waves with Comparisons to Linear Tidal Data	
	5b. GRANT NUMBER
	5c. PROGRAM ELEMENT NUMBER
	0602435N

6. AUTHOR(S)	5d. PROJECT NUMBER
Jim Hawkins, Alex C. Warn-Varnas, I. Christov	
	5e. TASK NUMBER
	5f. WORK UNIT NUMBER
	73-6838-A7-5

7. PERFORMING ORGANIZATION NAME(S) AND ADDRESS(ES)	8. PERFORMING ORGANIZATION REPORT NUMBER
Naval Research Laboratory Oeeanography Division Stennis Spaee Center, MS 39529-5004	NRL/BC/7320-07-7278

9. SPONSORING/MONITORING AGENCY NAME(S) AND ADDRESS(ES)	10. SPONSOR/MONITOR'S ACRONYM(S)
Office of Naval Research 800 N. Quincy St. Arlington, VA 22217-5660	ONR
	11. SPONSOR/MONITOR'S REPORT NUMBER(S)

12. DISTRIBUTION/AVAILABILITY STATEMENT

Approved for publie release, distribution is unlimi

20091021254

13. SUPPLEMENTARY NOTES

14. ABSTRACT

Analysis of tides and internal waves from model studies in the South China Sea is done using three techniques. We summarize results from standard Fourier methods, continuous wavelet analysis and the direct seattering transform. Because the Fourier and wavelet analysis are inherently linear methods their utility in application to nonlinear dynamics is often questioned. Nevertheless, they have shown to be useful in delineating first order dynamics (for example finding fundamental modes). On the other hand the seattering transform, sometimes described as a 'nonlinear Fourier' technique, can in some cases succeed in elucidating non-linear dynamics where linear methods have proven less successful. We apply these proeedures to model results from Lamb's 2D non-hydrostatic model applied to the South China Sea and in some cases the multi-component tides used to force the Lamb model.

15. SUBJECT TERMS

discrete fourier transform, eontinuous wavelet transform, direct scattering transform, Luyon strait, Internal gravity waves

16. SECURITY CLASSIFICATION OF:			17. LIMITATION OF ABSTRACT	18. NUMBER OF PAGES	19a. NAME OF RESPONSIBLE PERSON
a. REPORT	b. ABSTRACT	c. THIS PAGE	UL	23	Alex Warn-Varnas
Unclassified	Unclassified	Unclassified			**19b. TELEPHONE NUMBER** (Include area code) 228-688-5223

Fourier, Scattering, and Wavelet Transforms: Applications to Internal Gravity Waves with Comparisons to Linear Tidal Data

James A. Hawkins[1], Alex Warn-Varnas[2], and Ivan Christov[2,3]

[1] Planning Systems Inc., Slidell, LA 70458, USA, jhawkins@psislidell.com
[2] Naval Research Laboratory, Stennis Space Center, MS, 39529, USA, varnas@nrlssc.navy.mil
[3] Northwestern University, Evanston, IL 60208, USA, christov@northwestern.edu

Abstract. Analysis of tides and internal waves from model studies in the South China Sea is done using three techniques. We summarize results from standard Fourier methods, continuous wavelet analysis and the direct scattering transform. Because the Fourier and wavelet analysis are inherently linear methods their utility in application to nonlinear dynamics is often questioned. Nevertheless, they have shown to be useful in delineating first order dynamics (for example finding fundamental modes). On the other hand the scattering transform, sometimes described as a 'nonlinear Fourier' technique, can in some cases succeed in elucidating nonlinear dynamics where linear methods have proven less successful. We apply these procedures to model results from Lamb's 2D non-hydrostatic model applied to the South China Sea and in some cases the multi-component tides used to force the Lamb model.

Keywords: Discrete fourier transform, Continuous wavelet transform, Direct scattering transform, Luyon strait, Internal gravity waves

1 Introduction

It is widely accepted that the first recorded internal wave was that described by J. Scott Russel. The correct mathematical framework for the phenomena came later with Korteweg and de Vries and their description of the KdV solutions to the one dimensional problem (see [1]) for a brief account of the early history of internal waves). Oceanic internal waves arise because of the naturally occurring stratification of the ocean's water column. As a result, internal waves arise throughout the earth's oceans. Well known examples include the internal waves observed in the Strait of Gibraltar and in the Sulu Sea. The University of Delaware maintains a website (http://atlas.cms.udel.edu/) containing an exhaustive catalogue of internal wave images gathered by satellite

Internal gravity waves (IW) occur as a result of tidal flow over steep topography, for example, coastal shelves and deep water sills. As the tide flows over the topography the thermocline is depressed resulting in the generation of a bore. The bore propagates and its leading edge steepens through nonlinear effects. Thereafter, the bore degenerates into solitary waves through frequency and amplitude dispersion [1, 2].

Dispersive effects become increasingly evident as the IWs propagate, causing the amplitudes and number of oscillations to vary over time. In this sense IWs are non-stationary, that is their spatial and temporal scales change as the IWs develop.

Dispersion of IWs is commonly summarized in amplitude, wavelength, and velocity relations. For example the amplitude of a solitary wave depression can be plotted against its width (or half-width) over a range of propagation distances [3]. The amplitudes and widths are often obtained by inspection. While useful (and widely used) there remains some subjectivity involved in determining the participant values.

Objective analyses exist to investigate non-stationary processes. They include statistical methods such as principle component analysis and time-frequency analysis including Fourier techniques, wavelets and multiscale analysis. Recent studies have employed these tools to study a variety of problems (see for example [4]).

This paper describes in some detail the application of three techniques to modeling results for IWs generated in the Strait of Luzon and propagating into the South China Sea. They are (1) the discrete Fourier transform (DFT), the direct scattering transform (DST), and (3) the wavelet transform (WT). Furthermore, analysis of tidal data used in driving the IW model is included for comparison.

A good deal of interest exists concerning the generation and propagation of internal gravity waves in the South China Sea. As part of the Asian Seas Acoustics Experiment (ASIAEX), field measurements (encompassing a variety of platforms) took place in 2001 in South China Sea to quantify acoustic volume interaction during presence of solitary waves. Analysis of the field data showed the presence of solitary waves with amplitudes up to 160 m, and phase speeds of .83 m/s to 1.6 m/s [5]. The recent 2005 and 2006 Windy Island Experiment [6] measured amplitudes of up to 250 m and phase speeds up to 3.4 m/s. Recent modeling studies predict the occurrence of solitary waves consistent with those observed. The internal waves (IW) appear to be generated by deep water sills in the Luzon Strait. The IWs travel across the South China Sea towards the coast of China, their structure evolving as they propagate (see Fig. 1).

In the following the model predictions are discussed in Sect. 2. The analysis methods are briefly described in Sect. 3 in the following order, the DFT in Sect. 3.1, the DST in Sect. 3.2, and the WT in Sect. 3.3. Analysis of results are then discussed in Sect. 4. A concluding summary is contained in Sect. 5.
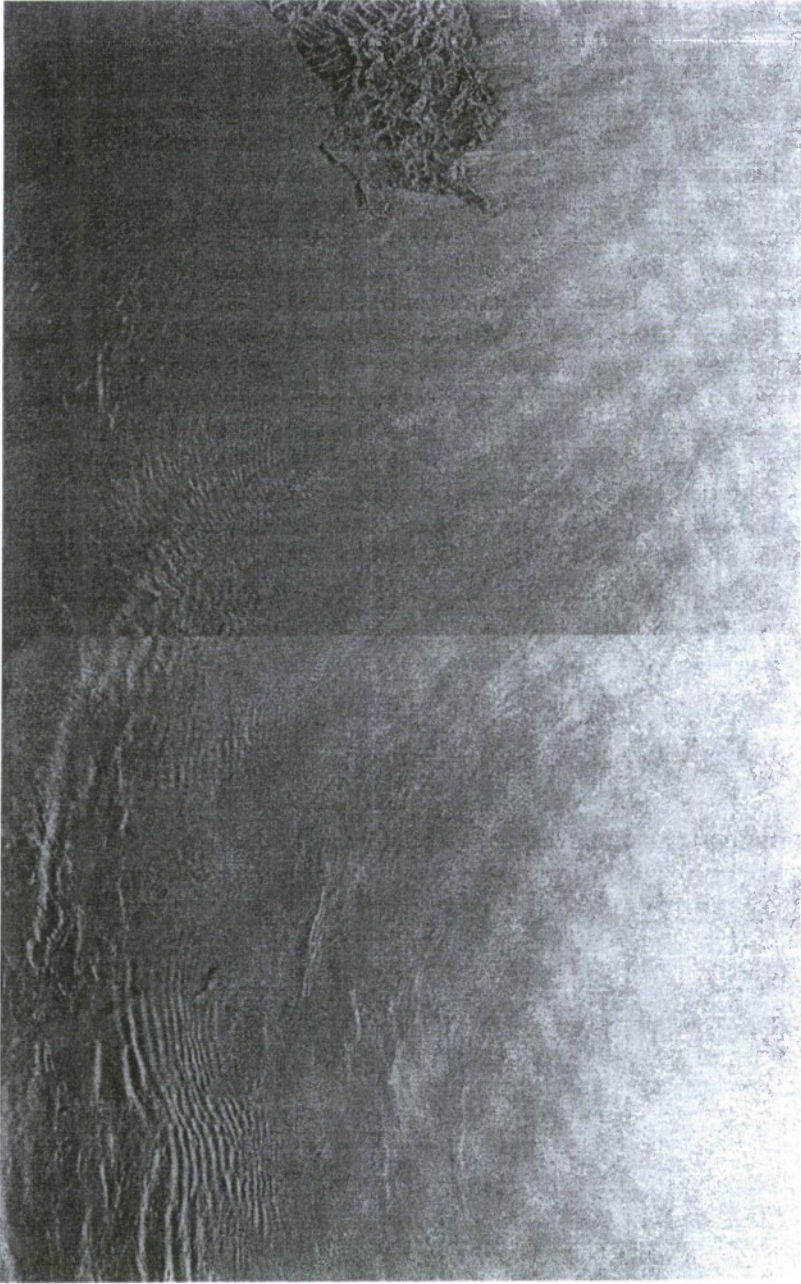
Fig. 1: Taiwan is located at the uppermost edge of the image. The Luzon Strait spans the region running south towards the Philippines (not shown) at the lower boundary. Internal waves can be seen in the lower left quadrant propagating westward (from University of Delaware, Center for Remote Sensing, url: atlas.cms.udel.edu).

2 Model Predictions

We have undertaken a model study of the area using the 2D ocean model developed by Kevin Lamb [2]. The model is initialized using analytic fits which approximate real density and bathymetry data. Internal waves are generated by tidal forcing from the Navy Coastal Prediction Model (NCOM) tidal model [7]. The results are discussed in the following paragraphs.

Figure 2 shows results from Lamb's 2D ocean model after 70 hours of simulation time. The density field is shown with several isopycnal lines spanning the domain of the upper 1000 m of ocean near the modeled sill of the Luzon Strait (the grey patch near the leftmost edge of the figure). Because the IWs described here begin as a tidal bore (a sharp depression of the pycnocline) and evolve into a group of solitary waves they can be identified throughout the domain as IW 'packets'. Three IW packets are easily noted located at ranges running east to west at −250 km, −550 km, and lastly near −700 km. The IWs are propagating toward a shelf located on the Chinese coast.

As the IWs propagate it is apparent that the nature of the IW packet is qualitatively changing over time. The IW at −250 km is tightly packed with numerous oscillations, at −550 km the oscillations have separated with large
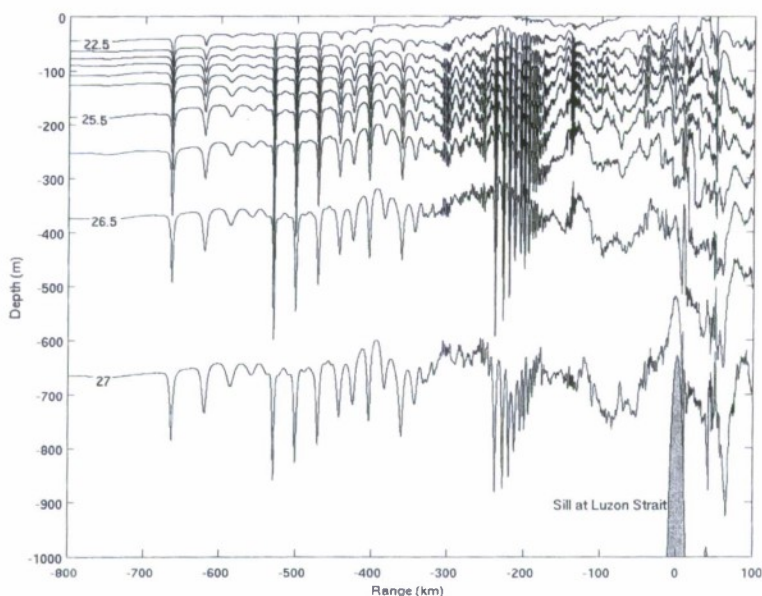

Fig. 2: Isopycnals (22.5–27, sigma-t units) are shown within the internal wave field. Results are from Lamb's 2D ocean model for the Luzon Strait.

amplitude oscillations at the leading edge of the IW packet, and still further at −700 km the separation continues, however the amplitude and number of oscillations has noticeably diminished.

The goal of the analysis in this paper is to compare the results from three techniques for quantifying the evolution of the internal waves. Each provides a different and complementary view of IW behavior.

3 Methods

In this section the techniques used for analysis are described. The DFT and WT are briefly summarized along with a more detailed development of the direct scattering transform. The descriptions here are provided as a point of reference for the discussion that follows. More detailed information can be found in the references.

3.1 Discrete Fourier Transform

An estimate of the energy or power at a particular Fourier frequency or wave-length characterizing a sequence is sought. First note that the squared value of a sequence integrated over time is a measure of energy. In this case we have the following expression for the energy, E, of a sequence $x(t)$ measured over time t with a period, L,

$$E = \int_0^L x(t)^2 dt. \tag{1}$$

The amount of power, W, in the sequence over the period is therefore given by the following equation,

$$P = \frac{1}{L} \int_0^L x(t)^2 dt. \tag{2}$$

The ideas above are implemented in a straight forward way by the *periodogram*. The discrete version of the periodogram, P_{xx}, can be written as follows [8],

$$P_{xx} = \frac{|X_L(f)|^2}{f_s L}, \tag{3}$$

where

$$X_L(f) = \sum_{n=0}^{L-1} x_L[n] \exp(-2\pi j f n / f_s), \tag{4}$$

is the discrete Fourier transform of the sequence $x(t)$ and f_s is the sampling frequency.

As will be seen in the following sections the DFT is more successfully applied to problems that are linear than to nonlinear problems like internal

waves. This leads one to speculate that perhaps a 'nonlinear' Fourier approach would prove more successful. The direct scattering transform is sometimes thought of as a nonlinear Fourier method in the sense that it uncovers constituent components in nonlinear problems.

3.2 Direct Scattering Transform

Next, we turn to the relationship between the (periodic, inverse) scattering transform and the (ordinary) Fourier transform, the interpretation of the former as a nonlinear generalization of the latter, and the algorithm for computing the DST spectrum of a data set. To this end, we begin by formulating the Korteweg–de Vries (KdV) equation, which describes the dynamics of weakly-nonlinear dispersive waves, for the internal-waves problem.

Under the assumption that the internal solitary waves are 'long' and that they are traveling in a 'shallow' layer (this will be made more precise below), the governing (KdV) equation of the pycnocline displacement, which we denote by $\eta(x, t)$, is

$$\eta_t + e_0\eta_x + \alpha\eta\eta_x + \beta\eta_{xxx} = 0, \quad 0 \leq x \leq L, \quad t \geq 0, \tag{5}$$

where $L(> 0)$ is the spatial period (i.e., the length of the domain), and the subscripts denote partial differentiation with respect to an independent variable. In addition, $c_0(> 0)$, $\alpha(< 0)$, and $\beta(> 0)$ are (constant) physical parameters (see, e.g., Apel [1] for their interpretation). The simplest way to evaluate them is to assume a two-layer (density) stratification [9]. Then we have

$$c_0^2 \simeq g\left(\frac{\varrho_2 - \varrho_1}{\varrho_1}\right)\left(\frac{h_1 h_2}{h_1 + h_2}\right), \quad \alpha \simeq \frac{3c_0}{2}\left(\frac{h_1 - h_2}{h_1 h_2}\right), \quad \beta \simeq \frac{c_0 h_1 h_2}{6}, \tag{6}$$

where h_1 and $h_2(> h_1)$ are the distances from the *unperturbed* pycnocline to the free surface and to the ocean bottom, respectively, while ϱ_1 and $\varrho_2(> \varrho_1)$ are the fluid densities in the top and bottom layers, respectively. Furthermore, we are interested in the periodic initial-value problem. That is to say, given a data set $\eta(x, t = 0)$ such that $\eta(x + L, 0) = \eta(x, 0)$ for $0 \leq x \leq L$, we wish to determine its evolution $\eta(x, t)$ for $t > 0$.

The strategy for solving the periodic KdV equation by the scattering transform can be split into two distinct steps: the *direct problem* and the *inverse problem*. The former, which is termed the *direct scattering transform* (DST), consists of solving the Schrödinger eigenvalue problem

$$\{-\partial_{xx} - \kappa\,\eta(x, 0)\}\,\psi = \mathcal{E}\psi, \tag{7}$$

where $\kappa \equiv \alpha/(6\beta)$ is a nonlinearity-to-dispersion ratio, ψ is an eigenfunction, and $\mathcal{E}$ is a (real) spectral eigenvalue such that $\sqrt{\mathcal{E}}$ is a (complex) wavenumber. For periodic signals, as we have assumed, it is well-known that the eigenvalues fall into two distinct sets [10]: the *main spectrum*, which we write as the set $\{\mathcal{E}_n\}_{n=0}^{2N}$, and the *auxiliary spectrum*, which we write as the set $\{\mu_n^0\}_{n=0}^{N-1}$,

On the other hand, the inverse problem consists of constructing the *nonlinear Fourier series* from the spectrum $\{\mathcal{E}_n\} \cup \{\mu_n^0\}$ using Abelian hyperelliptic functions [10] or the Riemann Θ-function [11]. In former case, which is the so-called μ-representation of the scattering transform, the *exact* solution of (5), subject to periodic boundary conditions, takes the form

$$\eta(x,t) = \frac{1}{\kappa} \left\{ 2 \sum_{n=0}^{N-1} \mu_n(x,t) - \sum_{n=0}^{2N} \mathcal{E}_n \right\}. \tag{8}$$

It is important to note that all *nonlinear* waves and their *nonlinear* interactions are accounted for in this *linear* superposition. Unfortunately, the computation of the nonlinear normal modes (i.e., the hyperelliptic functions $\mu_n(x,t)$, $0 \leq n \leq N-1$) is *highly* nontrivial; however, numerical approaches have been developed [12] and successfully used in practice [13, 14]. In addition, we note that the auxiliary spectrum, often referred to as the hyperelliptic function 'phases,' is such that $\mu_n^0 \equiv \mu_n(0,0)$ [10, 14].

Several special cases of (8) offer insight into why the latter is analogous to the (ordinary) Fourier series. In the small-amplitude limit, i.e., when $\max_{x,t} |\mu_n(x,t)| \ll 1$, we have $\mu_n(x,t) \sim \cos(x - \omega_n t + \phi_n)$, where ω_n is a frequency and ϕ_n a phase. Therefore, if we suppose that all the nonlinear normal modes fall in the small-amplitude limit, then (8) reduces to the ordinary Fourier series. This relationship is more than just an analogy, Osborne and Bergamasco [15] give a rigorous derivation of the (ordinary) Fourier transform from the scattering transform. Next, if there are no interactions, e.g., the spectrum consists of a single wave (i.e., $N = 1$), we have $\mu_0(x,t) = \mathrm{cn}^2(x - \omega_0 t + \phi_0 | m_0)$, which is a Jacobian elliptic function with modulus m_0. In fact, it is the well-known *cnoidal wave* solution of the periodic KdV equation [1].

For the hyperelliptic representation of the nonlinear Fourier series, given by (8), the wavenumbers are *commensurable* with those of the ordinary Fourier series, i.e., $k_n = 2\pi(n+1)/L$ ($0 \leq n \leq N-1$) [10, 13, 14]. However, this is not the only way to classify the nonlinear normal modes. One can use the 'elliptic modulus' (or, simply, modulus) m_n, termed the 'soliton index,' of each of the hyperelliptic functions, which can be computed from the discrete spectrum as

$$m_n = \frac{\mathcal{E}_{2n+2} - \mathcal{E}_{2n+1}}{\mathcal{E}_{2n+2} - \mathcal{E}_{2n}}, \quad 0 \leq n \leq N-1. \tag{9}$$

Then, each nonlinear normal modes falls into one of three distinct categories based on its soliton index:

1. $m_n \geq 0.99 \Rightarrow$ solitons, in particular, $\mathrm{cn}^2(x|m=1) = \mathrm{sech}^2(x)$;
2. $m_n \geq 0.5 \Rightarrow$ nonlinearly interacting cnoidal waves (e.g., moderate-amplitude Stokes waves);
3. $m_n \ll 1.0 \Rightarrow$ radiation, in particular, $\mathrm{cn}^2(x|m=0) = \cos^2(x)$.

Furthermore, it can be shown [13, 14] that the amplitudes of the hyperel-

$$A_n = \begin{cases} \frac{2}{\kappa}(\mathcal{E}_{\text{ref}} - \mathcal{E}_{2n+1}), & \text{for solitons;} \\ \frac{1}{2\kappa}(\mathcal{E}_{2n+2} - \mathcal{E}_{2n+1}), & \text{otherwise (radiation);} \end{cases} \qquad (10)$$

where $\mathcal{E}_{\text{ref}} = \mathcal{E}_{2n^*+2}$ is the *soliton reference level* with n^* being the largest n for which $m_n \geq 0.99$. Then, clearly, the number of solitons in the spectrum is $N_{\text{sol}} \equiv n^*$.

To summarize: the DST consists of computing the amplitudes and degrees of nonlinearity (moduli) of the nonlinear normal modes. Furthermore, if the KdV equation governs (at least to a good approximation) the evolution of the data set, then the DST spectrum characterizes the dynamics for *all* time. If that is not case, then the DST provides an instantaneous projection of the dynamics onto the solution space of the periodic KdV equation, giving us a nonlinear characterization of the data set at a particular *instant* of time.

In addition, the DST has been successfully employed in the Fourier-like decomposition of data from inherently nonlinear physical phenomena such as shallow-water ocean surface waves [13], laboratory-generated surface waves [14], and internal gravity waves in a stratified fluid [16]. Also, we note that the numerical implementation of the DST used in this paper is a modified version of Osborne's automatic algorithm [10], as described in [17].

Finally, we quantify the assumption of 'long, shallow-water' waves made above, so that the limits of the DST's applicability are clear. The latter assumption amounts to requiring that the largest wave amplitude (denoted by $\eta_{\max} \equiv \max_{x,t} |\eta(x,t)|$) is much smaller than the top layer's depth, i.e., $\eta_{\max}/h_1 \ll 1$, and that the characteristic width of the waves is much greater than the top layer's depth, i.e., $h_1/\Delta \ll 1$, where Δ can be taken to be, e.g., the largest half-width of the waves [1, 9]. Also, we may compute the (spatial) Ursell number of a data set, which is defined [14] as

$$\text{Ur} = \frac{3}{16\pi^2} \left(\frac{\eta_{\max}}{h_2} \right) \left(\frac{L}{h_2} \right)^2. \qquad (11)$$

This gives an additional measure of the 'nonlinearity' of a wave train, with $\text{Ur} \simeq 1$ being the limit of linear theory.

3.3 Wavelet Transform

While characterizing the scale of internal waves is important, it is equally important to know how that scale changes over time. In this regard the wavelet transform proves particularly useful. Here we discuss the application of the continuous wavelet transform and leave aside other multiscale analysis which can be useful in analyzing IW [18]. The general development of the continuous wavelet transform is well described in the literature [19, 20].

The wavelet transform $W_g(s, x)$ of a spatial sequence $f(x)$ can be defined as follows,

$$W_g(s, x) = \int g_{sx'}(x) f(x') dx', \qquad (12)$$

where the wavelets $g_{sx'}(x)$ are generated from the shifted and scaled versions of the *mother wavelet* $g(x)$,

$$g_{sx'}(x) = \frac{1}{\sqrt{s}} g \left(\frac{x - x'}{s} \right), \tag{13}$$

where s and x' are real values that scale and shift the wavelet, respectively. Note that the wavelet transform is in fact a convolution of the wavelet g with the sequence $f(x)$.

In the work described here the continuous wavelet transform is used with the mother wavelet chosen to be the Morlet wavelet. This provides two advantages. First, as noted above the WT is a convolution of the wavelet with the sequence to be analyzed. Thus, the WT can be implemented using the convolution property of the Fourier transform, that is, convolution in space becomes a product of transforms in Fourier space. This property is employed in the algorithm described by Torrence and Compo [21] which is used here. In this formulation the discrete wavelet transform is the inverse Fourier transform of the following product,

$$W_n(s) = \sum_{j=0}^{N-1} \hat{f}_j \hat{g}^*(sk_j) \exp(ik_j n \delta x), \tag{14}$$

where $\hat{f}$ and $\hat{g}$ are the Fourier transforms of the sequence and wavelet, respectively. The second advantage the Morlet wavelet affords is that there is an explicit relationship between the wavelet scale s of a sequence and the standard Fourier components. This allows a direct comparison between the familiar DFT Fourier components and those obtained via the wavelet transform. The power of a wavelet component W_n is given by the amplitude squared $|W_n(s)|^2$.

4 Analysis

The analytic methods just described can be applied to both linear and nonlinear problems. We discuss application to linear problems using tide data and to nonlinear problems using internal waves.

Results from analysis of the data here can be grouped into two broad regimes. Characteristic scales can be discerned over illustrative segments of data which are short compared to the complete data set. Other patterns can only be made out if relatively long sequences are examined. Hence, in the following the analysis is divided into short and long data sequences. First, we investigate short segments of data in Sect. 4.1 and then longer data segments in Sect. 4.2.

4.1 Analysis: Short Data Sequences

In this section we look at the frequency and spatial characteristics of short data segments using the DFT, DST, and WT.

4.1.1 DFT

For analysis, we use several datasets. First, we will look at DFT analysis of tidal velocities. This data is linear and is a good example of the strength of the DFT. We will then analyze a segment of the internal wave shown in Fig. 2 using the DFT, the DST, and the wavelet transform. Finally, we will analyze a longer segment of the IW field using the windowed DFT and the WT and compare the results.

First consider the tidal velocity over time (days) and its Fourier spectrum shown in Fig. 3. The upper panel shows tidal velocity taken from the NCOM tides model [7] sampled at roughly an hour (59 mins) over about 50 days. Qualitatively, we see many high frequency oscillations on the order of a day and a long (14 day) component modulating the entire time period. The lower panel is the power spectrum of the sequence. Note the large amplitudes near 0.04 and 0.08 (h^{-1}), these components correspond to 12.4 and 24 hr tidal components as expected. The long (14 day) modulation component is the so-called fortnight effect known to exist in this tide and can be seen very near the left edge of the plot.

The DFT results for the tidal velocity clearly show the tide's component parts and are a good example of the utility of the DFT. In this case, tidal velocity, the dynamics are very nearly linear and hence it is a good candidate for analysis with the DFT.

We now consider a segment of the internal wave field from Fig. 2. In the upper panel of Fig. 4 the segment shows the oscillating displacement of a single isopycnal (25.1 in sigma units) which is near a depth of -150 m when undisturbed and includes 8 distinguishable troughs, the largest of which at -530 km reaching nearly -400 m. The segment is restricted to include only the internal wave 'packet' spanning a range between -550 km and -350 km. Here and in the coming discussion we will repeatedly examine this internal wave segment by a number of techniques. The lower panel shows the Fourier spectrum for the IW. It can be seen by inspection that the separation of the troughs of the IW in the upper panel are on the order of 25 km. The DFT spectrum shows the tides's Fourier components unevenly spread over a range near 25 km. This moderate spectral resolution giving the power in a range of components rather than clear peaks presents a limitation in the application of the DFT to IWs. The Welch spectrum is overlayed on the periodogram for comparison. While smoother, it nevertheless suffers the same problem with resolution.
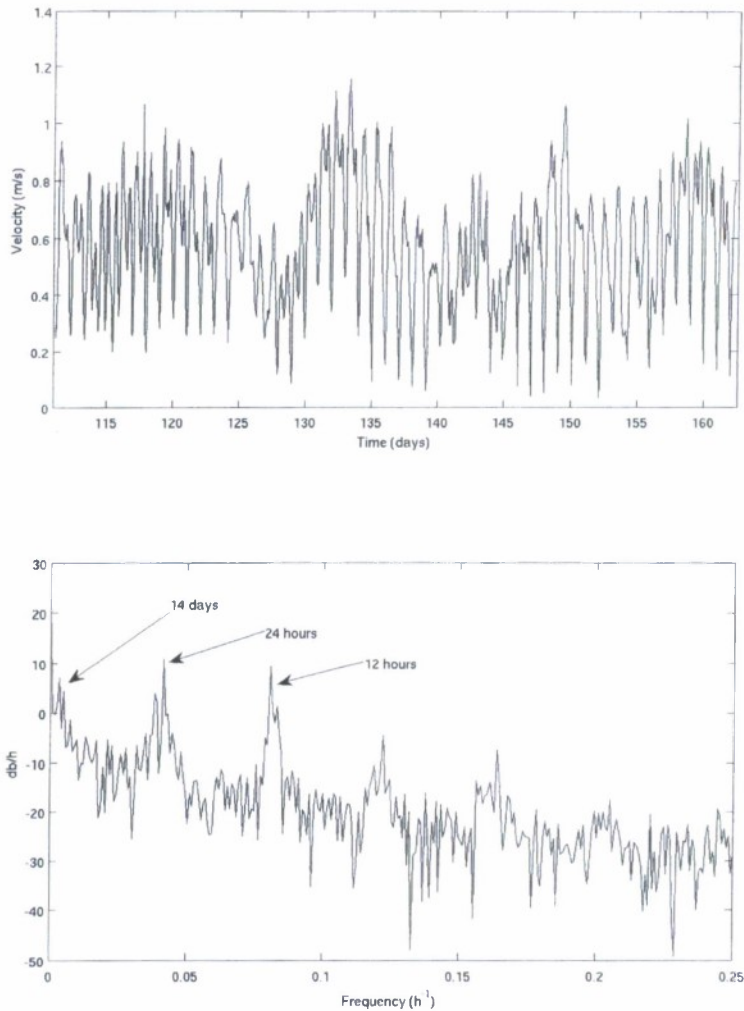
Fig. 3: *Upper panel* shows average tidal velocity in the Luzon Strait. The *lower panel* shows the Fourier components for the tide obtained from the DFT.

4.1.2 DST

Because of the physical basis of the DST, it only makes sense to apply it to nonlinear wave phenomena that are governed (at least to a good approxima-tion) by the KdV equation. Therefore, we only consider the application of the
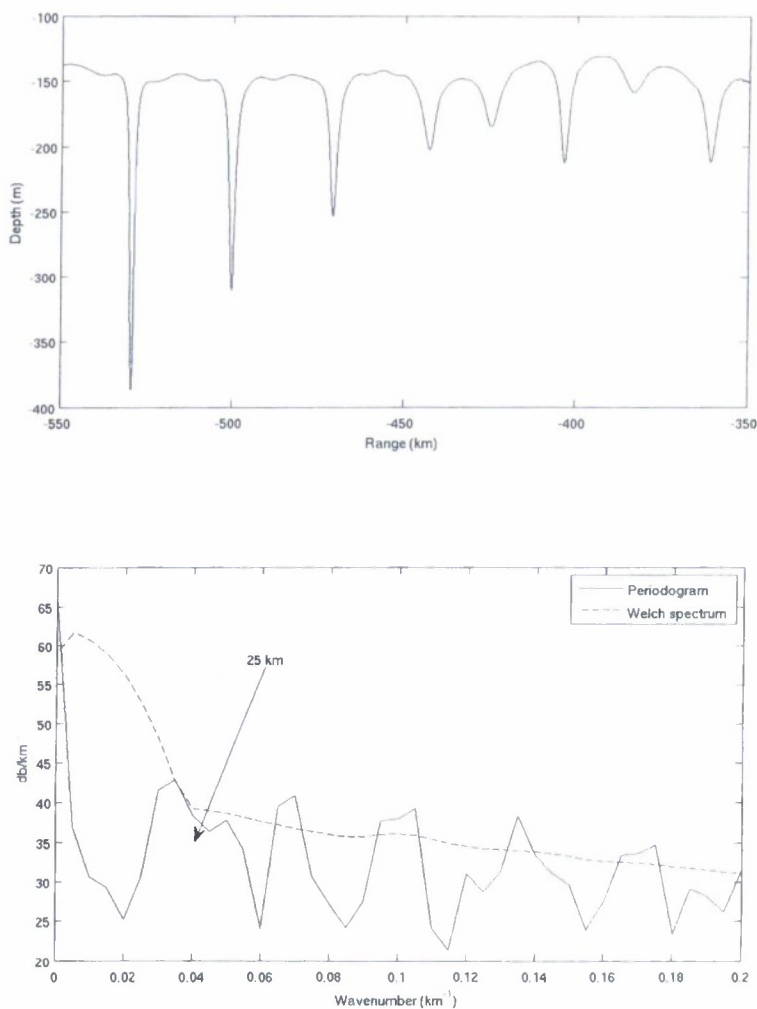
Fig. 4: *Upper panel* shows short segment of IW field taken from Fig. 1. *Lower panel* shows Fourier components calculated from the DFT. The periodogram (*solid curve*) and the Welch spectrum (*dashed curve*) are shown for comparison. Note that 25 km component 'disappears' as a result of smoothing the Welch spectrum.
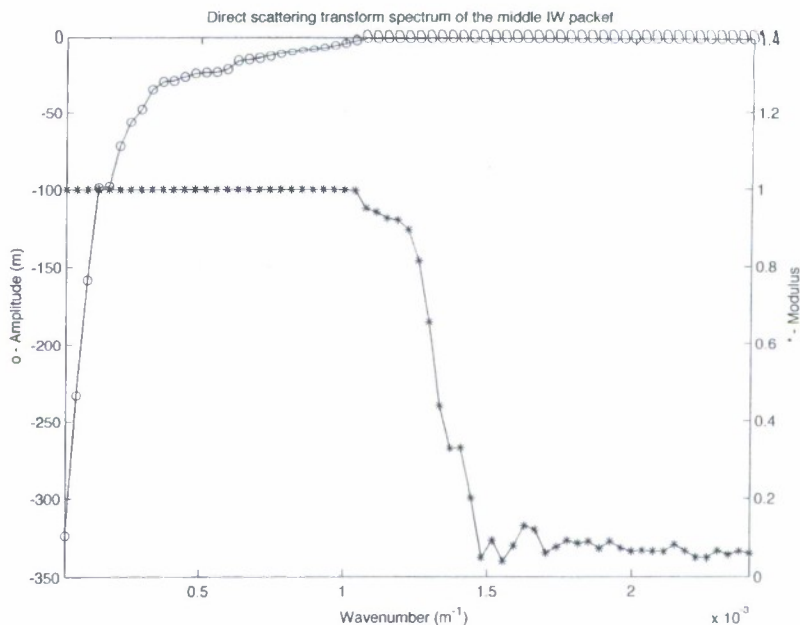
Fig. 5: Scattering transform spectrum of the middle wave packet (range -375 km to -545 km).

DST to the internal wave segment. The spectrum of the middle wave packet (recall Fig. 2) is shown in Fig. 5.

The DST finds 28 solitons in the data set traveling on a 'reference level' of -158.8 m; the Ursell number is 3.209. Physically, the reference level (shown as a black, dashed horizontal line in Fig. 5 and those that follow below) can be understood as the location of the undisturbed isopycnal in the absence of anything but non-interacting (well-separated) solitons. All this means is that the amplitudes of the soliton nonlinear oscillation modes are measured with respect to this reference level.

What is interesting about the DST spectrum is that it not only immediately captures the six solitary waves visible in the data set but also finds a number of 'hidden' modes that cannot be found by observation. Moreover, the DST spectrum reveals that the visible solitary waves fall into two distinct groups — the leftmost three waves and the one near -405 km form one group, while the ones near -445 and -425 km are part of another group. We can make this distinction because of the *trends* in the amplitude versus wavenumber plot of the spectrum given in Fig. 5. In other words, we see that the first four amplitudes' absolute values decrease essentially linearly with the wavenumber, and the slope of the line connecting them is about that of the line which connects the the crests of the leftmost three waves (and the one

near −405 km if it is 'moved' to be next to the latter ones). However, after the fourth mode in the spectrum, the trend of the nonlinear oscillations' amplitudes changes abruptly, which signifies a break in the pattern, and the rest of the modes cannot be grouped with the first four.

It may be surprising that there are 28 solitons in the spectrum of this wave packet, thus, one must keep in mind that these internal waves are highly nonlinear structures, while the KdV equation, which is the basis of the DST, governs the weakly-nonlinear limit. Therefore, we cannot say with certainty that there are *precisely* 28 solitons present in the data. However, we *can*, with a high degree of certainty, conclude that there are 'hidden' solitons and that solitons represent the energetic part of the spectrum (i.e., moderately nonlinear waves and radiation are hardly present, if at all).

4.1.3 WT

Here we will consider the wavelet transform of the IW segment previously discussed shown in the upper panel of Fig. 4 (the WT of tidal data will be considered in a later section). The results are shown in Fig. 6. Note that the x-axis duplicates that shown with the data sequence (between −550 and −350). In this sense the spectrum power is co-located near it's associated IW. The y-axis shows the Fourier wavelength associated with the wavelet scale. The
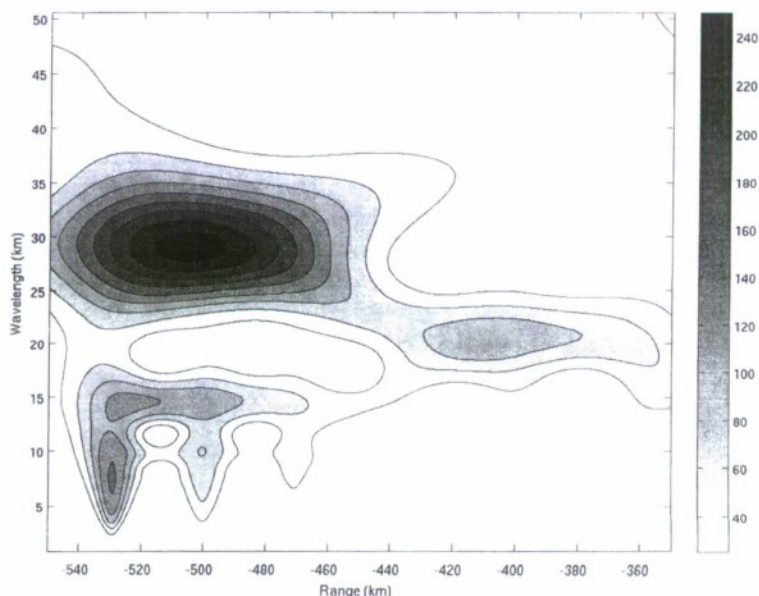

Fig. 6: Wavelet spectrum for internal wave segment. *Darker colors* represent greater

spectrum shows components with significant energy spread over the region between −460 km and −540 km peaking near −510 km at a wavelength of near 30 km. The location of these components indicates that the primary characteristic lengths associated with the first few depressions are about 30 km.

Note small increased areas of wavelet power near the ranges −530 km, −500 km, −470 km. These components are associated with individual troughs of the IW. This can be understood by recalling that the wavelet transform is a convolution of the wavelet with the waveform being analyzed. These small peaks come about when the probing wavelet becomes situated inside the IW troughs. As a consequence, the wavelet scale is on the order of the width of the troughs of IW. This feature is not observed with the DFT.

The great advantage that the continuous wavelet transform enjoys is the ability to isolate the characteristic scales of IW. While the resolution is not to the extent that we have seen in the Fourier analysis of the tidal data (Fig. 3), nevertheless, the WT is able to locate the characteristic scales of IWs. Moreover, the WT localizes these scales in space. This feature holds the possibility that the scale of the IW can be tracked over time. This phenomenon is investigated more closely in the following sections.
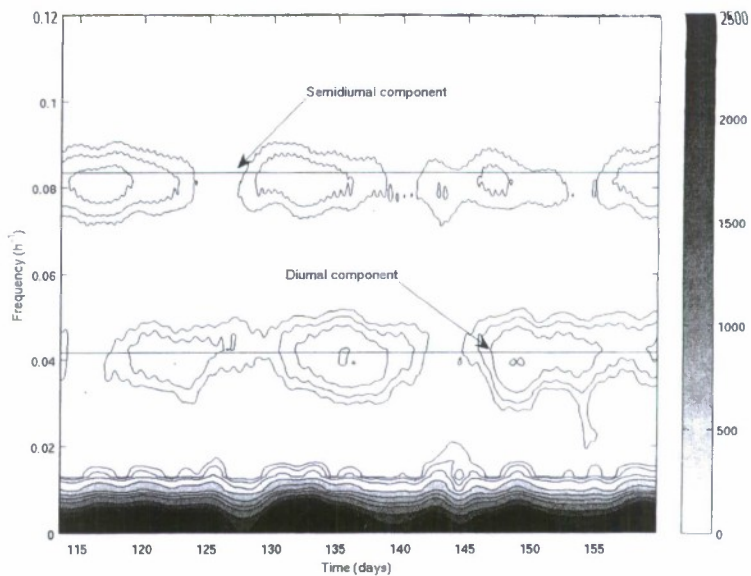
4.2 Analysis: Long Data Sequences

As previously noted, internal waves are nonstationary in the sense that their characteristic spatial and temporal scales evolve over time. At its inception the IW packet is a single depression (or bore) in the isopycnal, which, upon propagation developes into a series of solitary waves through nonlinear dispersion. These solitons grow in amplitude and separate, effectively lengthening the packet. The fully developed IW packet analyzed in the above sections is of this type. Further propagation leads to an IW packet whose constituent solitons has diminished in both number and amplitude. Thus, the three IW packets observed in Fig. 2 can be thought of as snapshots of a single IW packet over its lifetime. This pattern is repeated to varying degrees in most naturally observed IWs. The evolutionary aspect of IW dynamics is a good example of a nonstationary system. For this reason, it is instructive to investigate long data sequences to elucidate this behavior.
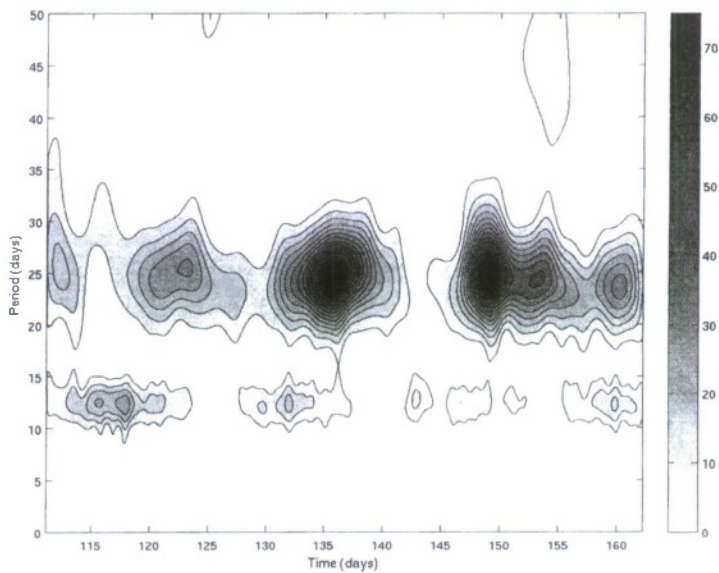
In the following section, the windowed discrete Fourier transform is used to investigate tidal data. Subsequently, the long data sequence of the IW field is analyzed with the WT and and the DST.

4.2.1 Windowed Discrete Fourier Transform

We noted earlier that the DFT does not discern variations in time in the sense that the components discovered via the DFT occurred throughout the tidal time sequence. Some resolution in time can be gained by repeatedly applying the DFT within a short window which is 'slid' along the waveform being analyzed. This is the idea behind the windowed Fourier transform (WFT). Fig. 7a shows the results of applying the WFT to tidal data obtained from

(a) Windowed Fourier transform of tidal data.

(b) Wavelet transform of tidal data.

Fig. 7: Tidal data analysis results: (a) windowed Fourier transform (b) wavelet
transform. *Darker colours indicate greater correlation.*

NCOM and used to drive the Lamb model to generate internal waves. The x-axis is time and ranges over about 50 days and the y-axis is the usual Fourier frequency (h^{-1}). With the spectrogram we can see variation over time of the frequency components of the tide. There are at least two peaks in the spectrum, one at 0.04 and another at 0.08 (h^{-1}) associated with 12.4 and 24 hr tidal period respectively. In analysis of the tidal data the WFT yields good time-frequency information.

4.2.2 Wavelet Transform

The wavelet transform can be considered a refinement of the WFT. Recall that the mother wavelet is scaled and shifted along the waveform to be tested yielding the wavelet spectrum. In this sense the WFT represents a crude wavelet which is a square wave that can be scaled and shifted along the waveform, the resulting spectrum varying with both time and frequency. Noting this similarity it is not surprising that, we expect the wavelet transform to yield results similar to those of the spectrogram.

Figure 7b shows the wavelet transform for the tidal data previously analyzed. Again we can make out the diurnal and semi-diurnal components of the tide. Qualitatively, the results are almost identical to those found using the WFT (excepting that the WFT returns the reciprocal of the period).

Lastly we consider a series of three internal wave packets and analyze the result with wavelets. In Fig. 8 the upper panel shows the series of IWs and the lower panel the associated wavelet spectrum. The results show the generation and evolution of the internal wave packets as they propagate toward the leftmost edge of the domain.

The general features we saw previously (Fig. 6) are repeated for each of the packets (the middle packet being the one previously described). The peaks in the spectrum most closely associated with the leading edge of each of the IW packets, $(-670$ km, -500 km, -225 km) correspond to the characteristic wavelengths of the individual IW packets. The length increases from about 10 km for the first packet to about 30 km for the middle packet and roughly 35 km as the packet reaches the left boundary. The increase reflects the gradual increase in distance between troughs within each packet.

Referring to the peaks in the wavelet spectrum allows us to draw attention to the wavelet component with the maximum intensity. However the peaks are surrounded by areas of high (relative to the background) intensity reflecting the fact that the spectrum is spread across wavelengths and ranges. In Fig. 8 the concentration of spectral intensity 'spreads' with time so that we see the intensity of the spectrum for the IW packet at -225 km is well concentrated in range and wavelength, at -500 km the intensity measurably broadens and finally the intensity of the packet at -670 km is quite diffuse. The cause of this general dissipation could be from attenuation of the internal wave packet through either physical or numerical mechanisms.
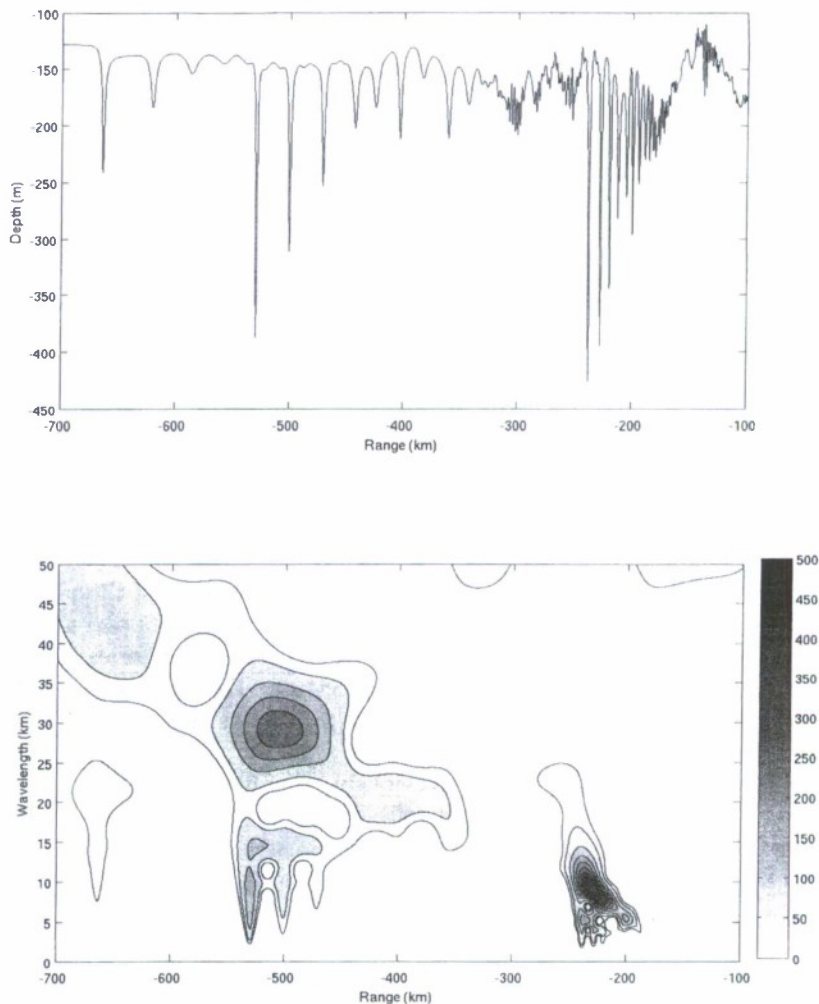
Fig. 8: Wavelet transform spectrum for long time internal wave sequence.

Finally note the peaks associated with individual troughs within each of the three packets where the wavelets 'fit' just inside the individual troughs. The characteristic wavelength for these troughs does not appear to change significantly over the propagation distance. This indicates the general shape of the troughs is somewhat constant throughout the domain.

4.2.3 Direct Scattering Transform

Because the DST identifies the KdV-based nonlinear normal modes of the data set and their evolution, it would only make sense to perform a DST analysis of the entire isopycnal if it were governed by the KdV equation. Clearly, that is not the case as the solitary waves can 'age'. Therefore, in this subsection, we perform a 'windowed' scattering transform analysis of the full data set. That is to say, we take three snapshots of the evolution of the internal solitary waves and compute the DST spectrum of each. This approach is similar to that of Zimmerman and Haarlemmer [16], who computed the DST spectrum of their data at different times in order to identify the nonlinear normal modes that are invariants of the motion (i.e., those that do not change in time).

To this end, in the top panel of Fig. 9, we show the DST analysis of the leftmost (farthest away from the sill) wave packet of the isopycnal under consideration. The middle wave packet, which was the subject of Sect. 3.2, is given in Fig. 5. And, the rightmost (closest to the sill) wave packet's DST spectrum is shown in the bottom panel of Fig. 9. For the leftmost packet, the DST finds 27 solitons traveling on a reference level of -151.3 m; the Ursell number of the data set is 2.008. On the other hand, for the rightmost wave
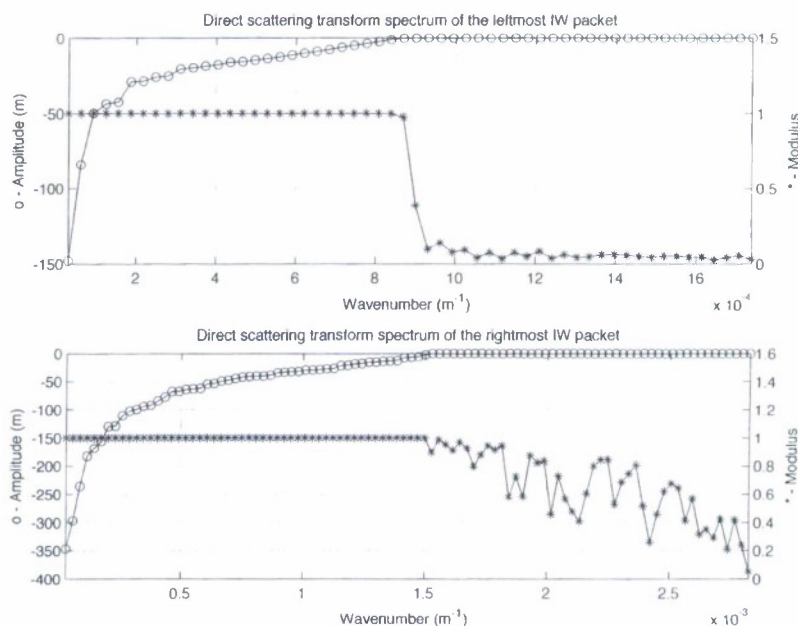

Fig. 9: *Top* and *bottom panels* display the scattering transform spectra of the leftmost (range -150 km to -368 km) and rightmost (range -547 km to -750 km) wave packets of the isopycnal under consideration.

packet, the DST finds 52 solitons traveling on a reference level of -163.9; the Ursell number is 5.718.

The first thing we notice is the similarity in the trend of the nonlinear normal modes' amplitudes (i.e., the rate of increase/decrease of the amplitudes with the wavenumber) in each snapshot. As was the case for the middle internal wave packet we discussed earlier, the largest amplitudes, which decrease quickly (in absolute value) with the wavenumber, are easily seen to be those of the solitary waves visible in the data set. Then, there is a large number of 'hidden' modes whose amplitudes' absolute values decrease approximately linearly with the wavenumber. Furthermore, the spectrum of each wave packet is clearly dominated by solitons, as the amplitudes of the nonlinear normal modes with moduli $m_n < 0.99$ are very small (in absolute value) in comparison with the soliton modes. Again, we emphasize that we cannot be certain whether there are precisely 52 or 28 solitons in the respective internal wave packets. Nonetheless, the DST provides concrete evidence of the nonlinear and *evolving* nature of the packets. Moreover, there is no doubt that solitons are the most prominent part of the spectra, and that their number decreases as the internal wave packets propagate away from the sill.

Furthermore, though for the first wave packet (see top panel of Fig. 9) the non-soliton normal modes are mostly radiation, as their moduli are $m_n \ll 1$, for the middle and rightmost wave packets (see Figs. 5 and bottom panel of 9) we observe more nonlinear normal modes to the right of the 'soliton cutoff' of approximately 1.3×10^{-3} m^{-1}. This correlates with the fact that the Ursell number of this wave packet is the largest of the three — almost twice that of the middle packet and three times that of the leftmost packet. Moreover, this result is consistent with the fact that farther away from the sill the internal waves are, the closer their dynamics are to the KdV (and, eventually, linear) ones.

5 Summary

Data and model studies of internal gravity waves show that their generation and evolution is accompanied by changes in their characteristic spatial and temporal scales. This nonstationary, dispersive behavior arises from nonlinear elements in IW dynamics. In IW studies, dispersion is commonly summarized in amplitude, wavelength, and velocity relationships. Often these are constructed by inspection. In the work described here, objective, analytic tools are employed to investigate the non-stationary behavior of IWs.

In this paper, three methods have been applied to internal wave data generated by Lamb's [2] model designed to simulate IWs observed in the Luzon Strait and South China Sea. They are the following: (1) the discrete Fourier transform, (2) the direct scattering transform and (3) the wavelet transform. The analysis has been applied to linear tide data, to 'short' internal wave data

and to 'long time' segments. Each method yields positive results which in some cases are complementary (DFT, WT) and in some cases unique (DST).

The DST allows for a truly nonlinear analysis of the internal waves and provides a measure of the applicability of the Korteweg-de Vries equation. While the DST does not necessarily give precise quantitative results that can be used for predictive purposes, it provides a 'genuinely nonlinear' decomposition of the data set. In particular, the DST spectra of the snapshots of a wave packet at different stages of its evolution allow us to see the 'nonlinear mode conversions' taking place over time and provides an understanding of solitary wave 'aging' in terms of these modes (notice the decrease in the number of nonlinear oscillation modes for wavenumbers between 0 and $\approx 5 \times 10^{-4}$).

The discrete Fourier transform, the windowed Fourier transform and the wavelet transform res present a continuum of Fourier based approaches to investigate IWs. Each yields the Fourier components of the internal waves and further, the WT (thought of in terms of a refined WFT) provides a view of how these modes change over time. In this regard, we have seen that the WT elucidates the evolving character of internal waves thus providing a time/frequency picture of the evolving dynamics of the internal wave over long periods.

In summary, each technique can be seen to provide positive recognizable details of IW dynamics. It is not uncommon to find that what is obvious to the naked eye cannot be verified by reasonable examination. Thus, while the results described in this paper fall short of a complete quantitative description of IW dynamics, nevertheless, that these methods support and expand on what can be seen 'by eye' is a nontrivial result. Certainly, the entire catalogue of analyses applicable to the investigation of internal waves has not been addressed here. However those described here represent a span of means by which to investigate internal wave dynamics. Moreover, it is reasonable to expect that further work will yield more quantitative results.

References

1. J. R. Apel: 2003. A new analytical model for internal solitons in the ocean. J. Phys. Oceanogr. **33**, 2247–2269.
2. K. G. Lamb: 1994. Numerical experiments of internal wave generation by strong tidal flow across a finite amplitude bank edge. J. Geophys. Res. **99**(C1), 843–864.
3. A. C. Warn-Varnas, S. A. Chin-Bing, D. B. King, Z. Hallock, and J. A. Hawkins: 2003. Ocean-acoustic solitary wave studies and predictions. Surveys in Geophysics. **24** 39–79.

4. A. Grinsted, J. Moore, and S. Jevrejeva: 2004. Application of the cross wavelet transform and wavelet coherence to geophysical time series, Nonlinear Processes in Geophysics **11**, 561–566.

5. T. F. Duda, J. F. Lynch, J. D. Irish, R. C. Beardsley, S. R. Ramp, and C.-S. Chiu: 2004. Internal tide and nonlinear wave behavior at the Continental Slope in the North China Sea. IEEE J. Ocean Eng. **29**, 1105–1130.

6. S. R. Ramp, 2006. Private communication.

7. S.-Y. Chao, D.-S. Ko, R.-C. Lien, and P.-T. Shaw: 2007. Assessing the West Ridge of Luzon Strait as an internal wave mediator. J. Oceanogr. **63** (No.6), 897–911.

8. Signal Processing Toolbox User's Guide for use with MATLAB. The Math-Works, Inc. (2002).

9. A.R. Osborne, T.L. Burch: 1980. Internal solitons in the Andaman Sea. Science **208**, 451–460.

10. A.R. Osborne: 1994. Automatic algorithm for the numerical inverse scattering transform of the Korteweg–de Vries equation. Math. Comput. Simul. **37**, 431–450.

11. A.R. Osborne, M. Serio, L. Bergamasco, and L. Cavaleri: 1998. Solitons, cnoidal waves and nonlinear interactions in shallow-water ocean surface waves. Physica D **123**, 64–81.

12. A.R. Osborne and E. Segre: 1991. Numerical solutions of the Korteweg–de Vries equation using the periodic scattering transform μ-representation. Physica D **44**, 575–604.

13. A.R. Osborne, E. Segre, G. Boffetta, and L. Calaveri: 1991. Soliton basis states in shallow-water ocean surface waves. Phys. Rev. Lett. **67**, 592–595.

14. A.R. Osborne and M. Petti: 1994. Laboratory-generated, shallow-water surface waves: analysis using the periodic, inverse scattering transform. Phys. Fluids **6**, 1727–1744.

15. A.R. Osborne and L. Bergamasco: The solitons of Zabusky and Kruskal revisited: perspective in terms of the periodic spectral transform. Physica D **18**, 26–46.

16. W.B. Zimmerman and G.W. Haarlemmer: 1999. Internal gravity waves: analysis using the the periodic, inverse scattering transform. Nonlin. Process. Geophys. **6**, 11–26.

17. I. Christov: 2008. Internal solitary waves in the ocean: analysis using the periodic, inverse scattering transform. Math. Comput. Simul., arXiv:0708.3421, (in press).

18. S. Jevrejeva, J. C. Moore, and A. Grinsted: 2003. Influence of the artic oscillation and El Niño-Southern Oscillation (ENSO) on ice condition in the Baltic Sea: The wavelet approach. J. Geophys. Res. **108**, D21, 4677–4688.

19. P. Kumar and E. Foufoula-Geogiou: 1994. Wavelet analysis in geophysics: an introduction. Wavelets in Geophysics, E. Foufoula-Georgiou and P. Kumar, eds. Academic Press, San Diego. pp. 1–45.

20. L.H. Kantha and C.A. Clayson: 2000. Appendix B: Wavelet Transforms. Numerical Models of Oceans and Oceanic Processes. L.H. Kantha and C.A. Clayson, eds. Academic Press, San Diego. pp. 786–818.

21. C. Torrence, G.P. Compo: 1998. A practical guide to wavelet analysis. Bull. Am. Met. Soc. **79**, 61–78.